JOURNAL OF MATERIALS SCIENCE 22 (1987) 1277–1285

Identification of boron in $M_{23}X_6$ precipitates in 316 stainless steel using electron energy loss spectroscopy

J. F. MANSFIELD
Electron Microscopy Centre for Materials Research, Materials Science Division, Argonne National Laboratory, Argonne, Illinois 60439, USA

AISI 316 stainless steel, which is frequently employed in the power industry, shows considerable increases in high-temperature creep ductility when small quantities of boron are added to it. However, considerable effort by a number of researchers has failed to reveal the exact location of the boron and the mechanism by which it enhances the creep properties. The work presented herein involved the study of two casts of 316 steel with varying boron concentrations. Low-resolution location of the boron was performed by secondary ion mass spectrometry. The boron was mostly segregated to the grain boundaries of the steel. Scanning electron microscopy (SEM) and transmission electron microscopy (TEM) revealed that the grain boundaries were heavily coated with precipitates of the carbide $M_{23}X_6$ (M = metal, X = C, B, N). These precipitates were identified by X-ray energy-dispersive spectroscopy, in both the TEM and SEM, and convergent-beam electron diffraction in the TEM. Electron energy loss spectroscopy was employed to locate the boron within the carbides. The visibility of the boron *K* edge was enhanced by a digital filtering technique. Detection of boron in the $M_{23}X_6$ precipitates has made it possible to re-evaluate previous work on this subject and the role of boron in the improvement of the creep ductility of stainless steel is suggested.

1. Introduction

The study of boron in iron and steel is over fifty years old. Initially boron was treated as a "trace impurity". It was observed to have both beneficial and detrimental effects upon the macroscopic properties of alloys, depending upon its concentration and distribution within the material. Current manufacturing techniques, however, now frequently involve the addition of small quantities of boron to an alloy to enhance specific properties, e.g. the hardenability of a ferritic steel [1] and the creep ductility of an austenitic alloy [2]. It is the effect of boron on creep ductility that is of particular interest in this work.

AISI 316 stainless steel have numerous applications in power generation plants, both conventional and nuclear because of their long-term high-temperature mechanical properties. Since 316 steel generally enters service in a solution-treated condition that is thermodynamically unstable, prolonged exposure to stress and high temperature results in a considerable amount of secondary phase formation. In order to determine how to tailor the alloy to specific needs a great deal of research has been conducted on this steel and a large body of information is now available on the microstructure and chemistry as a function of time, temperature and stress.

Although it is beyond the scope of this work to review the precipitation kinetics of 316 steel (and the reader is directed to a number of papers that deal with the subject [3–5]), the behaviour of 316 steel during high-temperature creep and ageing can be generalized. The temperature regime to which this alloy is most suited is between 600 and 800° C. At these temperatures carbides of the type $M_{23}X_6$ (M = metal, X = C, B, N) precipitate, first at high-angle grain boundaries, next on incoherent and coherent twin boundaries and then finally intragranularly on dislocations. When the carbide is well advanced in its formation, the alloy composition in the grain-boundary areas can be sufficiently modified to allow intermetallic phases such as Laves, sigma (σ) and chi (χ) to form. Whether these form by decarburization of the carbide or directly from the matrix is still a matter of contention [3, 4, 6, 7]. Formation of all of the precipitation is accelerated when the alloy is subject to external stress. The intermetallics are generally hard and brittle as compared with the matrix and they may play a role in the failure of the alloy in extended creep testing [4].

Although considerable, the work on 316 steel is not exhaustive and there still remain a number of areas where its behaviour is not understood. For example, the addition of small quantities of boron, 20 to 200 p.p.m. by weight, produces radical increases in the rupture ductility at high temperatures. The exact role that the boron plays in this enhancement has been the subject of much discussion over a number of years. The aim of this paper is to propose an explanation for the role of the boron.

0022–2461/87 $03.00 + .12

TABLE I Cast composition (wt %)

Element	Cast	
	R	S
Fe	66.55	66.78
Cr	17.60	17.20
Ni	11.60	11.55
Mo	2.69	2.63
Mn	1.32	1.39
Si	0.51	0.32
C	0.060	0.050
N	0.030	0.034
S	0.021	0.022
P	0.015	0.014
B	0.0001	0.0060
	Traces of Ti, V, O, Al Ca	

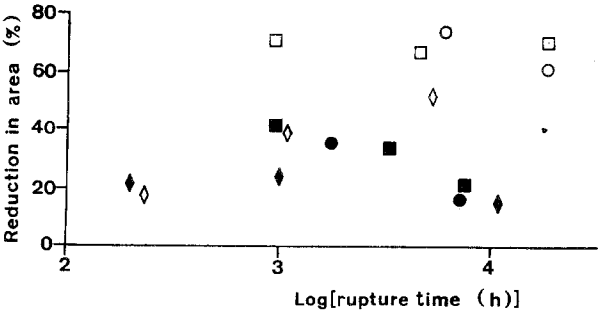

Figure 1 Graph illustrating the higher creep ductility exhibited by Cast S (open symbols) as compared to Cast R (filled symbols). (◇, ◆) 600° C; (□, ■) 650° C; (○, ●), 700° C.

2. Specimen history and experimental techniques

As part of their research into the properties of 316 steel the Electrical Research Association (ERA) and Berekeley Nuclear Laboratories (BNL) conducted extensive creep tests upon many different casts of the steel [8]. The results of these tests have been the subjects of correlation and regression analyses performed by several research groups [8–10]. The intention was to correlate how stress, temperature, grain size and composition affected the ductility of the material. While there was some disagreement as to the optimum method of analysis, several factors had strong effects on the ductility. Many of these could be readily explained. For example, sulphur and phosphorus were found to be deleterious. Both of these elements are frequently found to be segregated to grain boundaries, where they form compounds with the parent metals or precipitate elementally, each case being mechanically unfavourable. That the presence of boron in concentrations between 20 and 100 p.p.m. by weight was strong beneficial to the rupture ductility was less readily explainable.

In order to determine the role of the boron it was necessary to eliminate the effects of the other variables as far as possible. Hence study was confined to two casts of 316 steel taken from the ERA creep programme, which were, as far as possible, of identical composition except for their boron content. The casts had been labelled R (low boron) and S (high boron) by the ERA and this is how the samples will be referred to throughout this paper. The compositions of the casts are listed in Table I. Fig. 1 shows the results of extended creep tests of samples of R and S; the reduction in area of the gauge-length of the creep specimen, which is a measure of the ductility, is plotted as a function of time. The higher ductility of Cast S is clearly visible.

In order to determine how the microstructures of the casts developed during the creep tests a number of the creep samples were examined in the electron microscope. Pieces of solution-treated material were also examined to ensure that the original material was free from precipitation and large numbers of inclusions. Samples of the solution-treated alloy were aged at the same temperatures as the creep tests to compare the microstructures formed with and without applied stress. Samples were examined in both the SEM and TEM. SEM samples were mechanically polished and either chemically or ion-etched. TEM samples were produced by carbon extraction replication of etched and polished surfaces or by electrochemical thinning in a South Bay Technology jet-polishing machine (Temple City, California).

Chemical analysis in the SEM was performed by X-ray energy-dispersive spectroscopy (XEDS) and in the TEM by XEDS, convergent-beam electron diffraction (CBED), electron energy less spectroscopy (EELS) and selected-area diffusion. Analysis of the phases in the casts were simplified by comparisons with previously recorded data on 316 steel [11] and the use of "XEDS fingerprinting". Low resolution (to within 1 μm) location of the boron within the steel resulted from the application of direct-imaging ion microscopy. A Cameca secondary ion mass spectrometry (SIMS) instrument was used with a primary beam of 14.5 keV O_2^- ions. Images were recorded with both positive and negative secondary ions, permitting the location of many of the elements contained within the steel.

Higher resolution (to a few tens of nanometres) localization of the boron required the use of EELS; however, application of EELS to this problem was not straightforward. In EELS, the detection of light elements such as boron in a transition-metal matrix is usually difficult. The reason for this is the steeply sloping background in the spectra in the region from 100 to 300 eV. This background is largely due to the high-energy tails of transition metal M and N edges that occur in the 0 to 100 eV region of the spectra. Light-element K edges (e.g. boron 188 eV and beryllium 111 eV) are often obscured by this background. It is customary in EELS to remove the background by computer-modelling a window with a function of the form AE^{-r}, extrapolating the fit under the peak of interest and then subtracting the fit from the data to reveal the peak [12].

In the 100 to 300 eV region of spectra recorded from the $M_{23}X_6$ precipitates this background fitting procedure usually breaks down. Fig. 2 shows a partial EEL spectrum from an $M_{23}X_6$ precipitate in a grain boundary in an S sample with the background fits generated by a variety of possible background windows ranging from 30 to 110 eV below the energy of the boron K edge. None of the extrapolated background

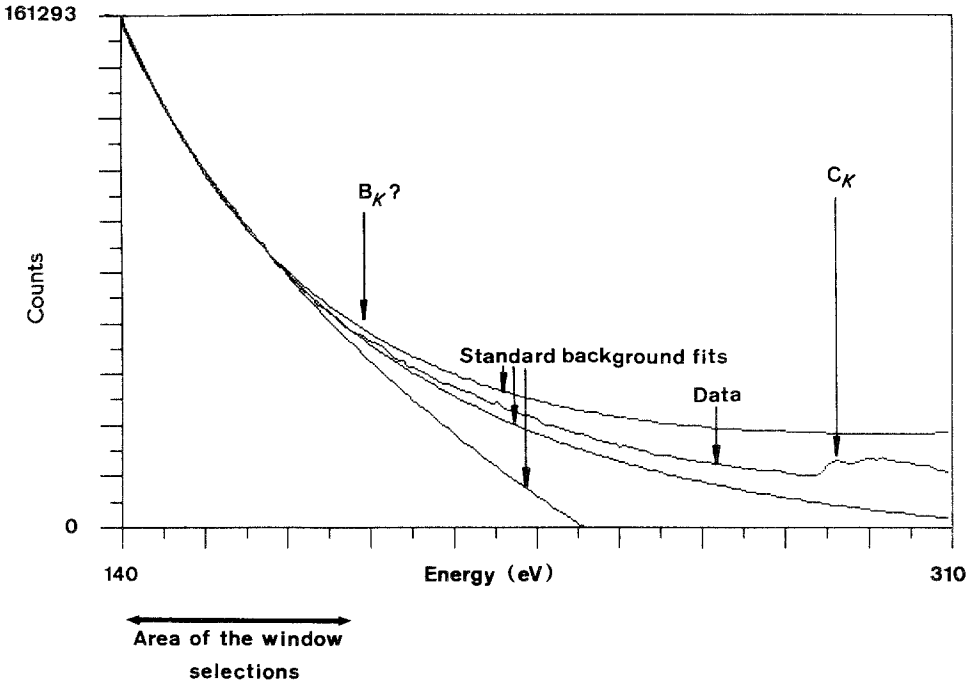

Figure 2 Partial as-recorded EEL spectrum from a precipitate of $M_{23}X_6$ in a sample of Cast S showing the failure of the AE^{-r} background model. Various background windows were tested; none were satisfactory.

fits are satisfactory and they could not be used to reveal unambiguously the boron *K* edge. In order to identify boron in these precipitates it was necessary to utilize a digital filtering technique developed by Zaluzec [13]. Symmetric zero-area digital filters with second-order top-hat profiles were used. The filtration essentially removes the background. The size and shape of filter required to reveal the presence of a weak light-element signal in a heavy matrix had been previously determined by Zaluzec and Mansfield [14].

3. Results and discussion

The solution-treated material contained virtually no precipitation and only occasional inclusions, e.g. manganese sulphide and some silicates. The high-boron cast did contain some examples of the boride M_3B_2. However, the aged and creep-tested material contained copious second-phase precipitation. Table II summarizes the major phases discovered and their locations. The findings were in good agreement with those of previous workers who analysed similar casts [3, 4, 15, 16]. The micrographs in Figs 3 to 6 are examples typical of the microstructures seen in the casts after long-term creep testing and represent a very small sample of the total number recorded in the characterization of the alloys. There was essentially no strong difference between samples of the two casts that had been subject to similar levels of stress and temperature. The presence or effect of the boron was not detectable in the microanalyses. It was evidently not responsible for any gross variation in the microstructure of the two casts.

The SIMS micrographs clearly showed that in both the R and S casts the boron was segregated to the grain boundaries. The micrographs in Fig. 7 are for creep-tested and aged samples of each alloy. The positive and negative ion micrographs are taken from different areas of the specimen. The use of SIMS here allowed only qualitative analysis of the boron. Quantitative analysis is possible; however, it is difficult in

TABLE II Results of the microstructural analyses of the two casts

Treatment	Cast	
	R (low boron)	S (high boron)
Solution-treated	Occasional manganese sulphides and silicate slags.	Scattered manganese sulphides and silicate slags.
Aged		
Medium term (5000 h)	$M_{23}X_6$ on grain boundaries, and twins.	$M_{23}X_6$ on grain boundaries and twins. Occasional M_3B_2 borides.
Long term (15 000 h)	$M_{23}X_6$ on grain boundaries, twins and intragranularly. Laves phase on boundaries and in grains.	$M_{23}X_6$ on boundaries, twins and in the grains. Laves phase on the boundaries and in grains.
Crept		
Medium term (5000 h)	$M_{23}X_6$ and Laves phase on boundaries and in grains.	$M_{23}X_6$ and Laves both inter- and intra-granularly.
Long term (15 000 h)	$M_{23}X_6$, Laves and sigma on boundaries. $M_{23}X_6$ and Laves in the grains.	$M_{23}X_6$, Laves and sigma on boundaries. Laves and $M_{23}X_6$ in the grains.

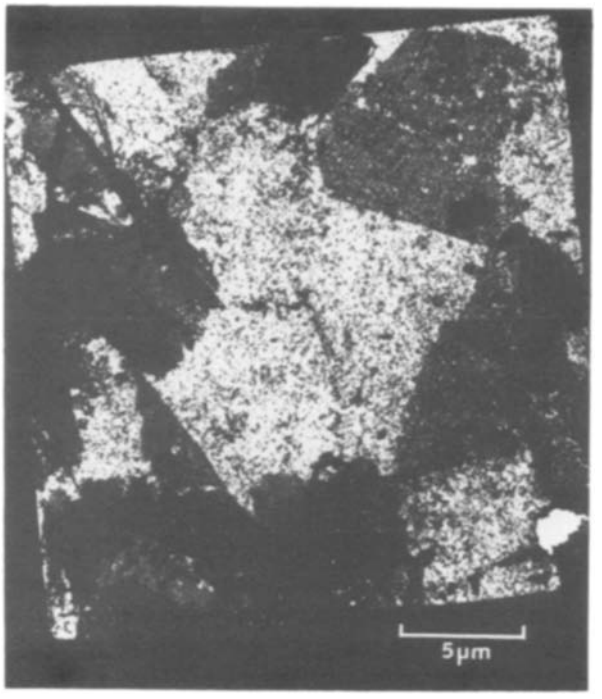

Figure 3 Sample R, crept at 600° C. An example of the copious precipitation that occurs in the samples during creep testing. This is a single grid square of a carbon extraction replica. The precipitates, both the continuous sheets and the discrete particles, are for the most part $M_{23}X_6$. The continuous sheets are thought to be extracted from the grain boundaries.

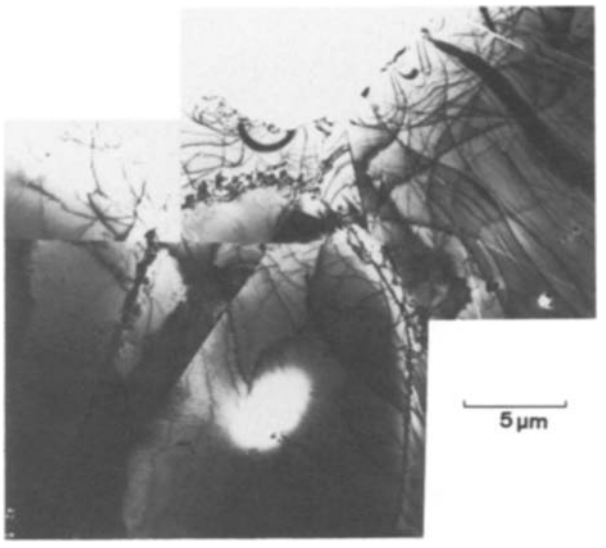

Figure 5 Sample S, crept at 600° C. Low-magnification micrograph of a thin foil of a creep specimen. There is copious grain-boundary precipitation and large numbers of dislocations.

such complex systems as 316 steel and hence the micrographs included are recorded under conditions that reveal each element most clearly. Variations in intensity from image to image cannot be used to infer changes in concentration. It can be seen that for the most part the carbon and boron are segregated to the austenite grain boundaries. The areas where there is a boron signal and no carbon are thought to indicate the presence of small borides, which are occasionally seen in the TEM. Note that molybdenum is also concentrated at the boundaries. Both carbon and molybdenum are known to be contained within the $M_{23}X_6$ carbides, and the molybdenum can be seen in the XEDS spectra (see Fig. 8); however, the spatial resolution of the SIMS images is insufficient to definitely conclude that the boron is also present in the carbides.

As an aside, it should be noted that the presence of molybdenum in these steels precludes the analysis of

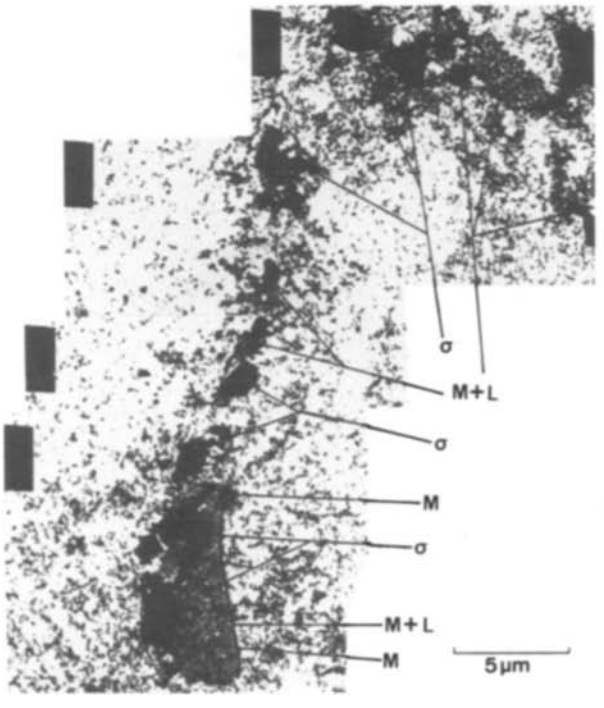

Figure 4 Sample R, crept at 600° C. A section of an extraction replica showing precipitates from a grain boundary. This sample had been crept for near 12 000 h and as a result there is a good deal of sigma phase (σ) and Laves phase (L) present with the $M_{23}X_6$ (M).

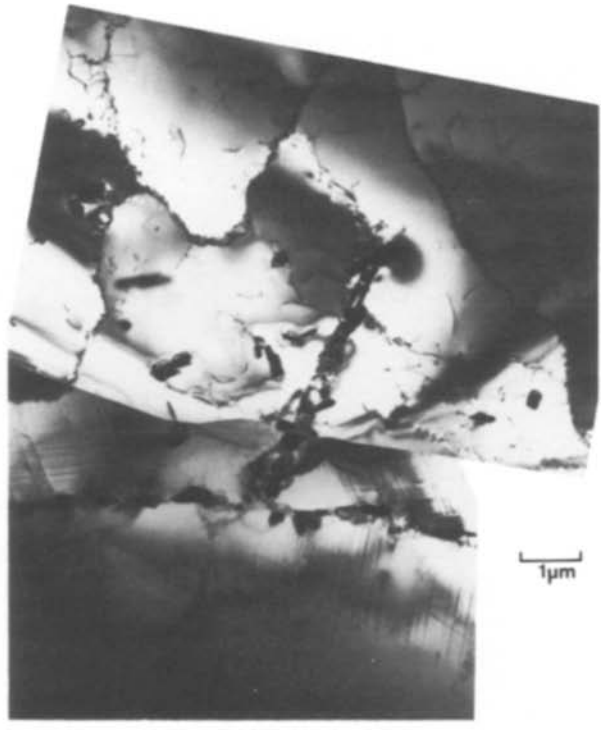

Figure 6 Sample S, crept at 600° C. Higher magnification micrograph of the same foil as Fig. 5. The dislocations can be seen to have formed sub-cells and the precipitation has not only coated the high-angle grain boundaries, but also the micro-twin in the centre of the picture and there is also some intragranular precipitation.

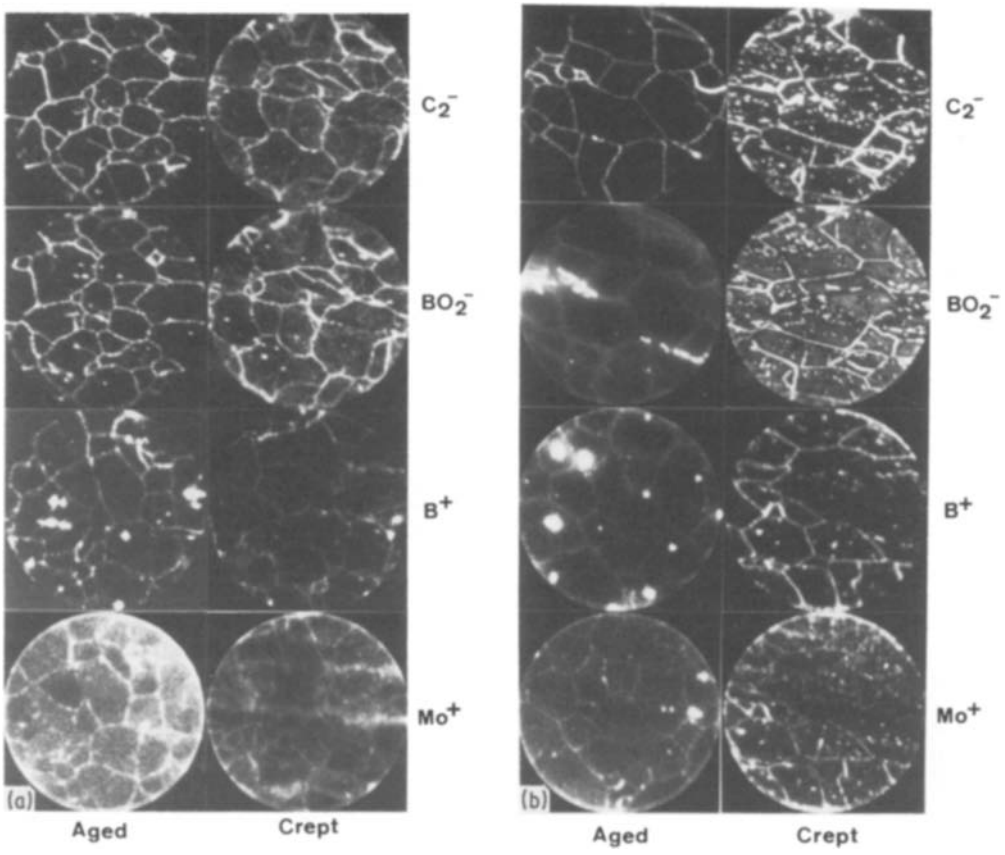

Figure 7 SIMS micrographs of creep-tested and aged samples from (a) Cast R and (b) Cast S. The boron and carbon signals are largely concentrated at the grain boundaries. There are a few cases where boron appears in the grains without an accompanying carbon signal; this is thought to indicate the presence of borides. Note the presence of molybdenum at the boundaries; this interferes with the analysis of the boron both in EELS and Auger spectroscopy. Areas are $\sim 200\,\mu m$ diameter.

these boundaries by low-temperature fracture and subsequent Auger analysis. Firstly, fracture at the grain boundaries is difficult due to the generally high ductility of 316. Secondly, the boron *KLL* lines are almost totally obscured by the molybdenum *MNN* lines [16]. EELS is the only technique that has the resolution required to refine the location of the boron.

Initially EELS experiments were performed on both extraction replicas and thin foils. It was observed that in extraction replicas the extra twenty or so nanometres specimen thickness of the carbon support film introduced sufficient multiple scattering in the 0 to 200 eV region of the spectrum to obscure the boron *K* edge even after digital filtering. Hence, all EELS spectra were recorded from electro polished thin foils. Since the SIMS results had indicated that the majority of the boron was located at the austenite grain boundaries in both the creep-tested and aged samples of each cast, most of the EELS work was performed on aged material as there was a much larger amount of it available. By selecting the polishing conditions so that the grain boundaries were preferentially attacked [17], it was possible to routinely produce thin foils with a number of carbide precipitates that were sufficiently thin for EELS analysis. Fig. 9 shows typical examples of the results of EELS analysis of the two casts. The raw data in each case do not give any indication whatsoever of the boron content of the precipitates. However, digital filtering with a second-order, zero-area top hat filter [14] reveals the boron *K* edge. In the S samples the boron edge was very obvious. However, in the R samples, although a feature was usually present in each R spectrum in the boron *K*-edge region, there was a degree of uncertainty in definitely indentifying it because it was not detectable above the residual noise level. Since the boron level is so much lower in the R cast this is not unreasonable. For comparison, a spectrum from the matrix of an R sample some distance from a grain boundary can be seen in Fig. 10, and no evidence of boron is visible. This spectrum was selected to illustrate the appearance of the "noise" in a section of the sample that should not contain boron. The origin of the noise is discussed further below. Spectra of the matrices of the two casts were usually indistinguishable.

It should be noted here that the application of the digital filtering technique is not trivial. There a number of points of which the experimenter should be aware. Firstly, the application of any digital filter to spectra will amplify any features which deviate from a smooth background. Thus, in addition to highlighting spectral edges, random noise is also exaggerated. Secondly, digital filters of the zero-area top-hat variety function ideally when applied to a signal with a linear background, where they will produce a filtered background with zero slope and amplitude. Where the background exhibits high curvature, as in the present spectra, it is necessary to include a pair of positive nodes in the filter to compensate; however, even with this type of second-order filter there can be anomalies. The apparent background noise in the filtered spectrum can sometimes appear to be high at low energy

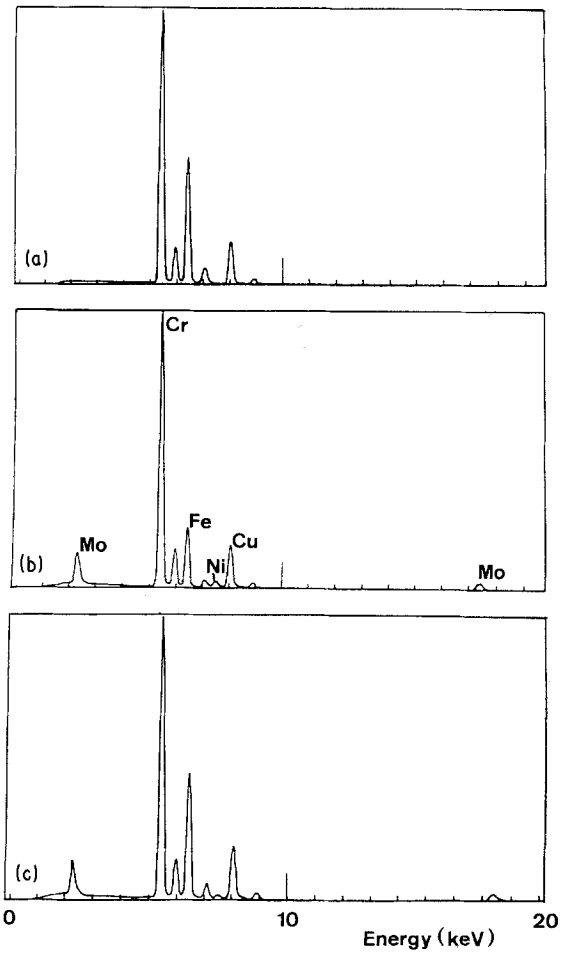

Figure 8 Characteristic XEDS spectra from typical $M_{23}X_6$ precipitates analysed in the samples in this study. The three spectra represent three different variants that were observed. Precipitates that gave rise to Spectrum (b) were most prevalent in both casts and constituted 90% of the particles analysed. There was no difference in composition between the two casts.

loss and decrease for higher losses. This is contrary to observations of an unfiltered spectrum, where the noise is more obvious at higher energy loss. It is my method of scaling the spectra for optimum observation of the areas of interest which makes the noise more obvious at lower count levels. The apparent decrease in noise with energy loss can be seen in the spectra in Fig. 9. In Fig. 9b (iv) there is also an artefact peak on the extreme left-hand edge of the spectrum. This feature is actually part of a series of oscillations that occur in the digitally filtered spectra when there is a change in gain from the pulse-counting mode at high energy loss to the analogue mode at low energy loss. The gain change is an abrupt change in signal over the range of a few channels and the filter treats it as a very large edge. In addition, the curvature of the spectrum background decreases with energy loss, which means that the filtered background becomes more linear with increasing loss. Quantification of digitally filtered spectra is not straightforward; it is necessary to produce standards for each element present, in much the same way that Auger spectra are quantified. Work is continuing to quantify the boron level in the S carbide.

Note that in the filtered $M_{23}X_6$ EEL spectra there are no molybdenum peaks labelled. The maximum amount of molybdenum in the precipitates is estimated, from the XEDS spectra, to be of the order of two atoms per formula unit. The only molybdenum peak that should be visible in the energy window of the spectra is the M_{45} peak. The energy of this edge is approximately 230 eV; however, it is usually observed to have a delayed maximum which occurs under, and is masked by, the strong carbon K edge. The carbon K edges in the spectra may therefore be partially $Mo_{M_{45}}$.

The concept that the boron is contained within the $M_{23}X_6$ carbides is not novel. Williams and Talks [18] and Matsuo *et al.* [19] reported that boron was incorporated into the $M_{23}X_6$ and gave rise to an increase in the lattice parameter. Both parties concluded that this increase resulted in a lower mismatch between the precipitate and the austenite matrix and an increase in the interfacial strength and hence the creep ductility. Henney and Jones [20] fabricated $M_{23}(C_{1-q}B_q)$, where q ranged from 1 to 6, and measured the lattice parameter by X-ray diffraction. They found that the lattice of the $M_{23}X_6$ increased for $q < 2$; when q was greater than 2 the resulting carbide was no longer a homogeneous solid and the lattice parameter remained approximately constant. In none of these cases was the boron definitely identified in the carbide matrix. In this work the boron has been found to be included in the carbide in the high-boron cast; however, it has not been possible to correlate the increase in lattice parameter. Attempts to measure the lattice parameter by CBED analysis using the positions of the higher-order Laue zone (HOLZ) lines were unsuccessful as the lines were usually sufficiently broadened by strains in the sample to preclude accurate determination of their positions [21].

A simple model of the grain structure of the steel was used to estimate the boron concentration in the carbides. The grains were assumed to be spheres with an average grain size which had been measured in the earlier work of Branch *et al.* [9] using standard optical metallographic methods. The precipitates of $M_{23}X_6$ were taken to be a shell around the grains of approximately 0.25 μm, this value being an average determined by measurement of carbides in the TEM. A matrix concentration of boron was calculated for both casts such that all the carbide would have two of its carbon atoms replaced by boron, i.e. to reach the "saturation" level discovered by Henney and Jones [20]. This value was compared with the actual concentration determined during the initial manufacture of the alloys. Elen and Glas [22] have shown that the solubility of boron in the matrix of 304L stainless steel was less than a few parts per million. Also, the strong segregation of boron to the austenite grain boundaries, which was evident even in the low-boron cast, indicated that the boron solubility in the matrix of the present casts was extremely low. The solubility of the boron in austenite was thus assumed to be negligible. A schematic diagram illustrating the grain model used in this estimate is shown in Fig. 11 and the results are shown in Table III. It was discovered that the S cast contained sufficient boron to "saturate" all of the grain-boundary carbide, whilst the R cast contained barely enough to reach 13% of saturation. An allowance was made for the occasional M_3B_2 borides

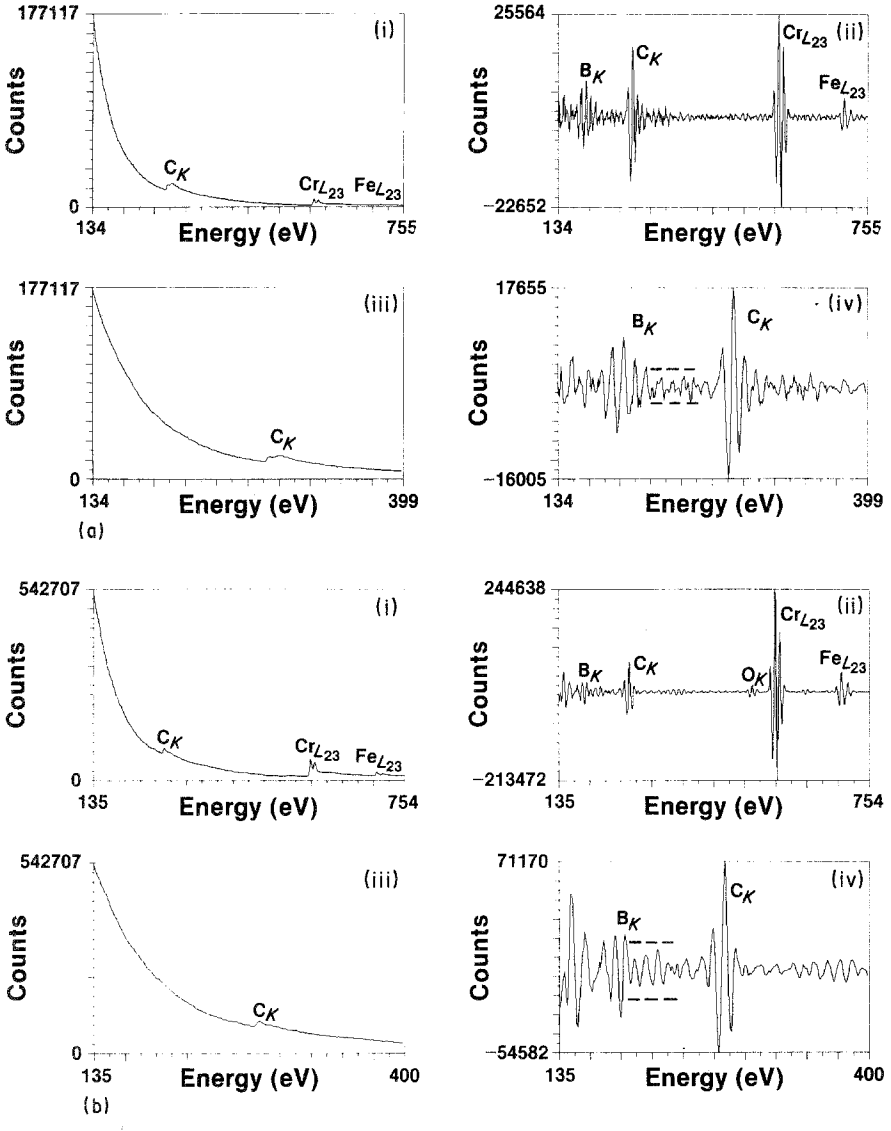

Figure 9 Partial EEL spectra of a typical ground boundary with $M_{23}X_6$ precipitates in specimens of (a) Cast S (0.006 wt % B) and (b) Cast R (0.001 wt % B): (i) showing the transition-metal L edges; (ii) the same area as (i) treated with a second-order top hat filter; (iii) the boron and carbon K edge region, raw data; (iv) as (iii), digitally filtered.

seen in the S cast, by assuming one 2 μm boride per average size grain ($\sim$22 μm); this allowance is an overestimate if one considers the number-density of borides seen in the TEM. This meant that the presence of the borides required a maximum matrix concentration of 0.001 wt %, hence there was still ample boron available to saturate the boundary carbide. In fact, it appeared that there would be a considerable amount in excess of that required to cause saturation. Although these estimates are very crude, they suggest that there may be some boron present at the matrix–carbide interface. This was also supported by the fact

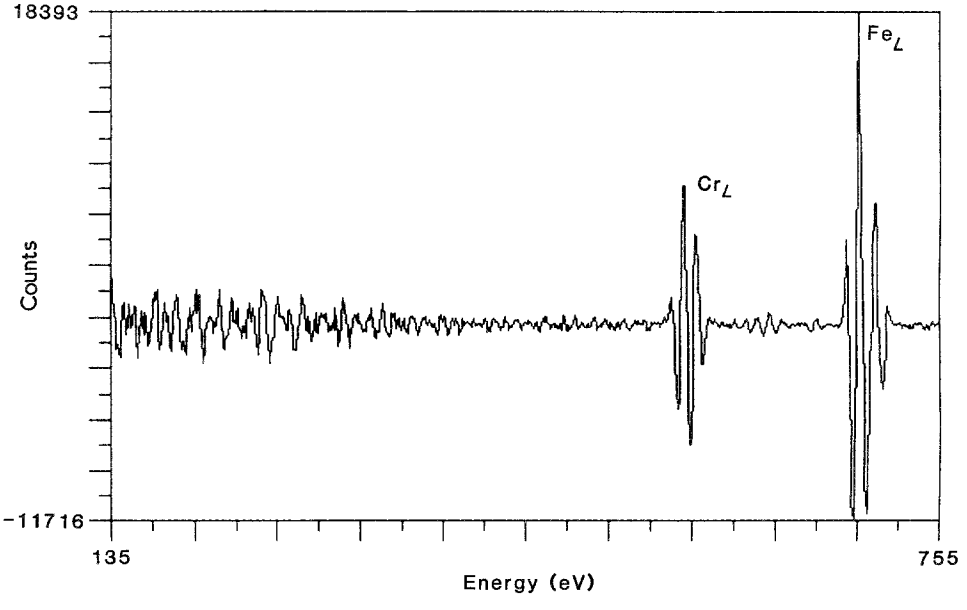

Figure 10 Partial EEL spectrum (digitally filtered) of the matrix of a typical sample of Cast R, for comparison with the spectra of the $M_{23}X_6$ precipitates. There is no discernible boron peak.

TABLE III Results of model calculations for $T = 0.25\,\mu m$ (see Fig. 11)*

	Cast R	Cast S
r (μm)	15.5	22.0
Matrix boron concentration (wt %)	0.0001	0.0060
Matrix boron concentration if carbide is saturated (wt %)	0.0008	0.0006

*Boron concentration in $Cr_{16}Fe_5Mo_2C_4B_2 = 0.016$ wt %.

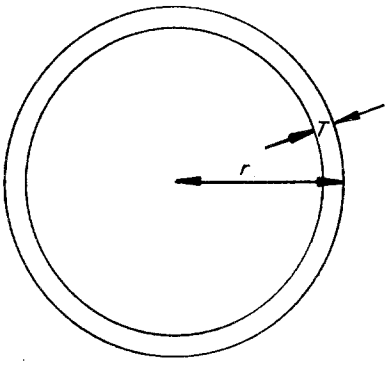

Figure 11 Schematic diagram of the simple model used to estimate the boron concentration of the grain-boundary precipitates together with the results obtained. The grain is approximated by a sphere in the precipitate matrix. The matrix concentration of boron was calculated assuming that the precipitate was saturated, i.e. two carbon atoms were substituted by boron. Results are given in Table III, T = precipitate 'shell thickness', R = mean grain size for each cast [9].

that the boron was seen in the SIMS micrographs to be nearly all segregated to the matrix grain boundaries. An attempt to confirm this experimentally involved digital EELS line-scans across matrix–precipitate interfaces. To date it has not been possible to detect any significant boron signal at these interfaces as probe size and signal levels are serious problems; however, work is continuing.

The reason for attempting to analyse for boron enrichment at the matrix–carbide interface is that it is possible that boron may play more than one role in its enhancement of the creep ductility. Although it is usually the case that elemental segregation to grain boundaries is detrimental to mechanical properties (as with sulphur and phosphorus), there have been occasions when such segregation has been beneficial [23, 24]. While there is at present no direct evidence that boron behaves in this manner, it remains a possibility. Future developments in microscope technology (higher voltage, smaller probe and higher beam current) may allow the solution of this question.

4. Conclusions

It has been shown that it is possible to detect boron in the presence of heavy transition metals by EELS when digital filtration is employed. Work is in progress to quantify the filtered spectra and the technique can be generalized to other materials.

Although it was not possible to measure the change in lattice parameter of the carbide in the electron microscope, it is not unreasonable to assume that this work is in agreement with that of Williams and Talks [18] and Matsuo *et al.* [19]. The boron, when present at sufficient concentrations, saturates the $M_{23}X_6$ by replacing two carbon atoms per unit cell. The resulting increase in lattice parameter means that the interface between the carbide and the matrix is strengthened, giving rise to enhanced creep lifetimes.

It is possible that the boron has more than one mechanism by which it improves the mechanical properties of 316 steel. In addition to entering the carbide $M_{23}X_6$, and increasing the lattice parameter, it can also be segregated to the matrix–precipitate interface where it may affect the motion of dislocations and so aid the ductility.

Acknowledgements

This work could not have been completed without the cooperation and support of a number of agencies. My thanks go to all involved. These include Peter Marshall, John Steeds, and Nestor Zaluzec for their help and suggestions throughout the work. Funding was provided by the Science and Engineering Research Council and the Central Electricity and Generating Board in the UK, and by the US Department of Energy, BES-Materials Sciences (Contract W-31-109-Eng-38). Specimens were furnished by the Electrical Research Association (Project Advisory Group 2021). The SIMS analysis was performed by Hans Odelius at Chalmers University of Technology at Goteborg, Sweden.

References

1. J. E. MORRAL and T. B. CAMERON, in Proceedings of International Symposium on Boron Steels (The Metals Society of AIME, 1980) p. 19.
2. G. HENRY, A. MERCIER, J. PLATEAU and J. HOFFMAN, *Rev. Met.* **60** (1963) 1221.
3. B. WEISS and R. STICKLER, *Met. Trans.* **3** (1972) 851.
4. J. K. L. LAI and A. WICKENS, *Acta Metall.* **27** (1979) 217.
5. J. K. L. LAI, *Mater Sci. Eng.* **61** (1983) 101.
6. H. J. GOLDSCHMIDT, "Interstitial Alloys" (Plenum, New York, 1967).
7. J. K. L. LAI and J. R. HAIGH, *Weld. J. Res. Suppl.* **58** (1979) 1s.
8. G. D. BRANCH, A. WICKENS and D. W. C. BAKER, in Proceedings of Conference on Creep Resistant Steels, Dusseldorf, West Germany (1972) Paper 9.3.
9. J. K. L. LAI, *J. Nucl. Mater.* **82** (1979) 123.
10. M. J. SHEEHAN and J. L. HENSHALL, Engineering Science Technical Note 81/11 (University of Exeter, UK, 1981).
11. J. MANSFIELD (ed.), "Convergent Beam Electron Diffraction of Alloy Phases" (Adam Hilger, Bristol, UK, 1984).
12. R. F. EGERTON, *Phil. Mag.* **31** (1975) 199.
13. N. J. ZALUZEC, *Ultramicroscopy* **18** (1985) 185.
14. N. J. ZALUZEC and J. F. MANSFIELD, Institute of Physics Conference Series No. 78 (Adam Hilger, Bristol, 1985) Ch. 6, p. 173.
15. N. S. EVANS, PhD thesis, University of Bristol UK (1980).
16. J. F. MANSFIELD, PhD thesis, University of Bristol, UK (1983).
17. B. J. KESTEL, "Polishing Methods for Metallic and Ceramic Transmission Electron Microscopy Specimens", Argonne National Laboratory Publication No. ANL-80-120 (Argonne National Laboratory, Illinois, 1981).
18. T. M. WILLIAMS and M. G. TALKS, *J. Iron Steel Inst.*

210 (1972) 870.
19. T. MATSUO, T. SHINODA and R. TANAKA, *Tetsu to Hagane* **69** (1973) 907.
20. J. HENNEY and J. W. S. JONES, AERE Report, AERE-R-9700 (Harwell, UK, 1980).
21. J. W. STEEDS, in "Introduction to Analytical Electron Microscopy", edited by J. J. Hren, J. I. Goldstein and D. C. Joy, (Plenum, New York, 1979) Ch. 15.
22. J. D. ELEN and A. GLAS, *J. Nucl. Mater.* **34** (1970) 182.
23. E. D. HONDROS and M. P. SEAH, *Int. Met. Rev.* **22** (1977) 262.
24. C. L. WHITE, L. HEATHERLY and R. A. PADGETT, *Acta Metall.* **31** (1983) 111.

Received 23 December 1985
and accepted 5 August 1986